

Reanalysis of $^{13}\text{N}(p, \gamma)^{14}\text{O}$ reaction and its role in stellar CNO cycle

S. B. Dubovichenko,^{1,2} R. Ya. Kezerashvili,^{3,4} N. A. Burkova,² A. V. Dzhezairov-Kakhramanov¹, and B. Beisenov^{1,2}

¹*Fesenkov Astrophysical Institute “NCSRT” ASA MDASI RK, 050020, Almaty, Kazakhstan*

²*al-Farabi Kazakh National University, 050040, Almaty, Kazakhstan*

³*New York City College of Technology, City University of New York, Brooklyn, NY 11201, USA*

⁴*Graduate School and University Center, City University of New York, New York 10016, USA*

(Dated: February 25, 2020)

Within the framework of the modified potential cluster model with forbidden states, the $^{13}\text{N}(p, \gamma)^{14}\text{O}$ reaction rate and the astrophysical S -factor are considered. It is shown that the first $p^{13}\text{N}$ resonance determines the S -factor and contributions of the $M1$ and $E2$ transitions are negligible at energies $E < 1$ MeV, but are significant at high energies. The S -factor strongly depends on the 3S_1 resonance parameters. The influence of the width of the 3S_1 resonance on S -factor is demonstrated. The reaction rate is calculated and an analytical approximation for the reaction rate is proposed. A comparison of our calculation with existing data is addressed. Results of our calculations for the $^{13}\text{N}(p, \gamma)^{14}\text{O}$ reaction rate provide the contribution to the steadily improving reaction rate database libraries. Our calculations of the $^{13}\text{N}(p, \gamma)^{14}\text{O}$ reaction rate along with results for the rates of $^{14}\text{N}(p, \gamma)^{15}\text{O}$ and $^{12}\text{C}(p, \gamma)^{13}\text{N}$ processes provide the temperature range $0.13 < T_9 < 0.97$ for the conversion of CNO cycle to the HCNO cycle. Our results demonstrate that at early stages of a nova explosion at temperatures about $0.1 T_9$ and at late stages of evolution of supermassive stars at temperatures about $1.0 T_9$ the ignition of the HCNO cycle could occur at much lower densities of a stellar medium.

PACS numbers:

I. INTRODUCTION

The radiative capture reactions play an important role in astrophysics. Light elements are either created during the big bang or during fusion reactions in stars. In the latter case, they are the result of hydrogen burning which are characterized by two major reaction sequences: i. the pp chain; ii. the carbon-nitrogen-oxygen (CNO) cycles [1]. The CNO cycle is considered as a catalytic process that requires the presence of some initial carbon, nitrogen, and oxygen abundance in the stellar material. Radiative capture reactions, namely those in which an atomic nucleus fuses with one proton or neutron and produces a nucleus with the emission of electromagnetic radiation, or with α -particle emission have of greatest importance in nuclear astrophysics [2, 3]. In particular, competing (p, γ) and (p, α) reactions are branching points in the CNO cycling process [1]. However, the strong-interaction (p, α) branch is substantially stronger than the electromagnetic (p, γ) branch, but, in some cases, the latter one can be comparable with the (p, α) , which alters the reaction flow substantially in certain astrophysical temperature regimes [4]. The proton induced radiative capture reactions (p, γ) occur in many stellar environments, for example, in novae and X -ray bursts. Especially, in stellar environments due to the high temperatures and short reaction times (p, γ) reactions involving short-lived nuclei play an important role for energy generation and nucleosynthesis. It takes the high-density environment of stars to generate nuclei with masses $A \geq 12$. The reactions of protons radiative capture are widely discussed in the literature (see reviews [2, 3, 5] and references herein). It is done primarily due to a fact that carbon component burns out in a series of processes known as hot CNO cycle (HCNO-I), which occurs at temperatures starting from $0.2 T_9$ [1]. The synthesized isotope ^{14}O is considered as a waiting point, which is overcome by a chain of reactions, starting with $^{14}\text{O}(\alpha, p)^{17}\text{F}$ when temperature is above $0.4 T_9$. The review [1] presents the comprehensive and consistent illustrations of CNO and HCNO-I cycle chains, as well as evolution of CNO isotope abundance with time for different density and temperature conditions, the calculations of which are directly based on the reaction rates.

The pioneering measurement with a rare-isotope beam was the first direct determination of the $^{13}\text{N}(p, \gamma)^{14}\text{O}$ reaction cross section using a radioactive ^{13}N beam [6–8]. In the reaction $^{13}\text{N}(p, \gamma)^{14}\text{O}$ the s -wave capture on the broad 1^- resonance dominates the reaction rate and over three decades many efforts have been made to determine the parameters for the resonance using different experimental approaches: transfer reactions [7, 9–11], Coulomb dissociation of high energy ^{14}O beam in the field of a heavy nucleus [12–14], a rare-isotope beam [6–8], using the unstable ion beam by indirect measurements [15, 16], and, the most recently, via neutron-knockout reactions with a fast ^{15}O beam [17]. Ref. [5] provides an overview of current experimental projects specializing in synthesis of radioactive isotope beams and experiments on astrophysical applications. However, today there is no experimental data suitable for comparison with theoretical calculations of cross sections or astrophysical S -factors. In this case, apparently, it is possible to synthesize isotope beams, given that its lifetime of 9.965 min is comparable with the neutron lifetime. At the same time, direct measurements of the reaction are carried out, although the isotope decays in 70.598 sec. Nevertheless, in

the future we can expect new data for the cross sections of the process $^{13}\text{N}(p, \gamma)^{14}\text{O}$ [5].

The results of the studies [6, 8, 15, 16, 18–24] on astrophysical S -factor and $^{13}\text{N}(p, \gamma)^{14}\text{O}$ reaction rate are included in the NACRE (Nuclear Astrophysics Compilation of REactions) database [25] and in the new compilation, referred to as NACRE II [26]. These databases form the basis for macroscopic astrophysical calculations. The key generalizing element of all calculations is the first 3S_1 resonance in the $p^{13}\text{N}$ scattering channel and all calculations are based on the energy and the width of this resonance. In the above mentioned works, experimental data on these characteristics are taken from Ajzenberg’s 1991 compilation [27]. At present, new data are available on the spectra of ^{14}O nucleus [28]. Therefore, it is relevant to consider these data for analysis of the $^{13}\text{N}(p, \gamma)^{14}\text{O}$ reaction. Moreover, another incentive for these calculations is the data from the latest experimental research [17] that will be also brought to our discussion.

Theoretical calculations of a reaction rate rely on the reaction cross section, which is determined by the nuclear structure of the nuclei involved, the reaction mechanism, and the associated interaction forces. The cross section can be calculated in the framework of *ab initio* models, where it is determined using the wave functions of the system, but subject to uncertainties associated with the theoretical model and the quality of the optical potential. Most notable are cluster model approaches, where nucleons are grouped in clusters of particles, which is a configuration that might, in particular, enhance the reaction rates and that rely on the quality of the optical potential [29–31]. Calculations of the rate for the $^{13}\text{N}(p, \gamma)^{14}\text{O}$ reaction and the astrophysical S -factor were performed within potential models using a shell-model, cluster model and R -matrix approaches [19–23]. There are significant differences between the various calculations of the $^{13}\text{N}(p, \gamma)^{14}\text{O}$ reaction as well as in the light of a new experimental study [17], an independent and well established approach is greatly needed to analyze this process. Continuing our studies of the processes of radiative capture on light atomic nuclei (see Refs. [29, 31, 33, 34] for concise summaries), we consider the reaction of $p+^{13}\text{N} \rightarrow ^{14}\text{O}+\gamma$ at astrophysical energies. This process is clearly not included in thermonuclear standard CNO cycle, but it makes a certain contribution to accumulation processes of a stable ^{14}N nucleus, which is further involved in other reactions of this cycle [35] and belongs to hot CNO cycle [1].

The goal of this study is twofold: i. to calculate the cross section of the $^{13}\text{N}(p, \gamma)^{14}\text{O}$ reaction at the energies of astrophysical interest and the reaction rate as a function of temperature for the analyses of the influence of the first $p^{13}\text{N}$ resonance width on the astrophysical S -factor; ii. to analyze and determine a temperature range for the conversion of the CNO cycle to the HCNO cycle.

The article is organized as follows. In Sec. II the potential cluster model with the classification of orbital states and methods of calculations are described. Classification and structure of states are introduced and analyzed in Sec. III, while in Sec. IV the potentials for the $p^{13}\text{N}$ interaction are presented. Astrophysical S -factor of the proton radiative capture on ^{13}N and the $^{13}\text{N}(p, \gamma)^{14}\text{O}$ reaction rate are given in Sec. V. The role of the $^{13}\text{N}(p, \gamma)^{14}\text{O}$ reaction in the conversion from the CNO to the hot CNO cycle is discussed in Sec. VI. Conclusions follow in Sec. VII.

II. THEORETICAL MODEL AND FORMALISM

To carry out calculations of astrophysical S -factors for various reactions, we usually use the modified potential cluster model (MPCM) of light atomic nuclei [29, 31–34] with the classification of orbital states according to Young diagrams [36, 37]. The model provides relatively many simple possibilities for performing calculations of various astrophysical characteristics. For example, one can calculate the astrophysical S -factor of radiative capture for electromagnetic transitions from scattering states of clusters to bound states (BS) of light atomic nuclei in cluster channels [29, 31]. The choice of this model is due to the fact that in many atomic nuclei the probability of cluster formation and the degree of their separation are relatively high. This is confirmed by numerous experimental data and various theoretical calculations obtained in various works over the past few decades [37].

Thermonuclear rates are defined by reaction cross sections which can be obtained using a theoretical model. In the present study of the $^{13}\text{N}(p, \gamma)^{14}\text{O}$ reaction we use the modified potential cluster model, where a proton interacts with a system of nucleons which are grouped into cluster ^{13}N . States of the $p-^{13}\text{N}$ system are defined by the classification according to Young diagrams. Relative motion wave functions are determined by solving the Schrödinger equation [29, 31–33]. The entry channel presents the proton $p(\frac{1}{2}^+)$ (J^π is the total momentum and parity) and $^{13}\text{N}(\frac{1}{2}^-)$ nucleus. For description of the final state we assume that ^{14}O nucleus consist of the same particles as in the input channel, but in the bound state.

In the microscopic formalism widely known as the resonating-group method [38, 39], the wave function of the $p^{13}\text{N}$ system has the form of an antisymmetrized product of internal cluster wave functions and a wave function of their relative motion:

$$\Psi = \hat{A}[\psi_p(\mathbf{r}_1)\psi^{13}\text{N}(\mathbf{r}_2)\chi(\mathbf{r}_1 - \mathbf{r}_2)]. \quad (1)$$

In Eq. (1) \hat{A} is the antisymmetrization operator, $\psi_p(\mathbf{r}_1)$ and $\psi_{^{13}\text{N}}(\mathbf{r}_2)$ are the wave functions of the proton and ^{13}N nucleus, respectively, \mathbf{r}_1 and \mathbf{r}_2 are the radius vectors of their center of mass, $\chi(\mathbf{r})$ is the wave function of their relative motion, while $\mathbf{r} = \mathbf{r}_1 - \mathbf{r}_2$.

According to [36, 38] the wave function of ^{13}N is antisymmetrized. Thus, only exchange transpositions between nucleons of the ^{13}N nucleus and proton must be taken into account which leads to the modification of the function. In contrast, in our approach this method of antisymmetrization, consists in the effective accounting of the Pauli principle by using the deep attractive potentials with the forbidden states (FS). Mathematically this realizes on the basis of classification of orbital states according to the Young diagrams [36, 37]. Exclusion of FSs from spectra leads to the correct node behavior of the function in the internal range, both for a bound state and for a continuous spectrum that, in its turn, reflects on the asymptotics of these functions.

To build interaction potentials between the proton and ^{13}N for scattering states in the MPCM, results of phase shift analysis of experimental data of differential cross sections for an elastic scattering of corresponding particles are usually used. The other way to build the potentials is to use spectra of the resulting nucleus ^{14}O [29, 31]. Moreover, the multiparticle nature of problem is taken into account by dividing a single-particle levels of such a potential into allowed and forbidden by Pauli principle [36, 37] states. The concept of Pauli-forbidden states allows one to take into account the multi-body character of the problem in terms of two-body interaction potential between clusters. For bound states (BS) of p and ^{13}N particles, potentials are built primarily on basis of the requirement to describe the main characteristics of the ^{14}O nucleus. For example, this is a requirement to reproduce the binding energy of ^{14}O in a corresponding $p^{13}\text{N}$ cluster channel and a description of the other static nuclear characteristics, such as a charge radius and asymptotic constant (AC), on its basis [32]. The functions of the initial input $p^{13}\text{N}$ and final ^{14}O output states are characterized by specific quantum numbers, including the Young diagrams f , which determine the permutation symmetry of the orbital part of relative motion wave functions of these states. Thus, the problem can be reduced to two parts:

- i. a construction of $p^{13}\text{N}$ interaction potentials with the FS for each partial wave, i.e., for the given orbital angular moment L , which also includes a point-like Coulomb term;
- ii. the numerical solution of the radial Schrödinger equation for these potentials to find the corresponding wave functions of the relative motion.

Further, following Refs. [29, 31], we use well-known expressions for total cross sections and matrix elements of multipole transition operators with the initial and final channel spins $S_i = S_f = S$

$$\sigma_c(NJ, J_f) = \frac{8\pi K e^2}{\hbar^2 k^3} \frac{\mu}{(2S_1 + 1)(2S_2 + 1)} \frac{J + 1}{J [(2J + 1)!!]^2} A_J^2(NJ, K) \sum_{L_i J_i} P_J^2(NJ, J_f, J_i) I_J^2(J_f, J_i), \quad (2)$$

where the notation NJ corresponds to EJ for the electric and MJ for the magnetic transitions, respectively. The matrix elements of the EJ transitions have a form

$$P_J^2(EJ, J_f, J_i) = (2J + 1)(2L_i + 1)(2J_i + 1)(2J_f + 1) (L_i 0 J 0 | L_f 0)^2 \left\{ \begin{matrix} L_i S J_i \\ J_f J L_f \end{matrix} \right\}^2 \quad (3)$$

and

$$A_J(EJ, K) = K^J \mu^J \left(\frac{Z_1}{m_1^J} + (-1)^J \frac{Z_2}{m_2^J} \right), \quad (4)$$

$$I_J(J_f, J_i) = \langle \chi_f | r^J | \chi_i \rangle. \quad (5)$$

In Eqs. (2) - (4) e is the elementary charge, $K = \frac{E_\gamma}{\hbar c}$ is the wave number of the emitted photon with energy E_γ , k is the wave number of particles in the initial channel, m_1, m_2 , and Z_1, Z_2 are masses and charges of colliding nuclei and μ is their reduced mass in the input channel, $S_i, S_f, L_i, L_f, J_i, J_f$ are the total spins, orbital momenta, total momenta of particles in the input (i) and output (f) channels, respectively, while $(L_i 0 J 0 | L_f 0)$ are the Clebsch – Gordan coefficients and $\left\{ \begin{matrix} \dots \\ \dots \end{matrix} \right\}$ are the $6j$ -symbols. The integral $I_J(J_f, J_i)$ is defined by using wave functions of relative motion of particles in the initial $\chi_i(r)$ and final $\chi_f(r)$ states, which depend on an intercluster distance r .

In the general form for MJ transitions for arbitrary rank J , the matrix element in Eq. (2) can be written using the $9j$ -symbols as

$$\begin{aligned}
P_J^2(MJ, J_f, J_i) &= S(S+1)(2S+1)(2J_i+1)(2L_i+1)(2J-1)(2J+1)(2J_f+1) \\
&\times (L_i 0 J - 10 | L_f 0)^2 \left\{ \begin{matrix} L_i J - 1 L_f \\ S & 1 & S \\ J_i & J & J_f \end{matrix} \right\}^2, \tag{6}
\end{aligned}$$

$$A_J(MJ, K) = \frac{\hbar K}{m_0 c} K^{J-1} \sqrt{J(2J+1)} \left[\mu_1 \left(\frac{m_2}{m} \right)^J + (-1)^J \mu_2 \left(\frac{m_1}{m} \right)^J \right], \tag{7}$$

$$I_J(J_f, J_i) = \langle \chi_f | r^{J-1} | \chi_i \rangle. \tag{8}$$

where m is a mass of a nucleus in output channel, μ_1 and μ_2 are magnetic momenta of the clusters, and the remaining notation are the same as in Eqs. (2) - (4).

Thus, to find the cross section of the $^{13}\text{N}(p, \gamma)^{14}\text{O}$ reaction one should calculate the expressions (5) and (8) for EJ and MJ transitions, respectively. The latter requires to find the radial wave functions χ_i and χ_f of relative motion of particles in the initial and final states.

III. CLASSIFICATION AND STRUCTURE OF STATES

Let us now consider a classification of $p^{13}\text{N}$ system orbital states according to the Young diagram. It was previously shown that the ground bound state (GS) of ^{13}N and ^{13}C nuclei corresponds to the Young orbital diagram $\{4441\}$ [36, 43]. Recall that possible Young's orbital diagrams in the system of $N = n_1 + n_2$ particles can be defined as a direct external product of the orbital diagrams of each subsystem [44], which for the $p^{13}\text{N}$ system within $1p$ shell gives $\{1\} \times \{4441\} \rightarrow \{5441\} + \{4442\}$. The first of the obtained diagrams is compatible with orbital momentum $L = 1, 3$ and is forbidden for the s -shell, since there cannot be five nucleons in the s -shell, while the second diagram is allowed and compatible with the orbital moments zero and two [44]. Thus, the potential of the 3S_1 wave has only the allowed state, but the P and F waves have both forbidden and allowed states [27]. However, since we do not have complete tables of the products of Young diagrams for a system with a number of particles greater than eight [45], which we used earlier for such calculations [29, 31], the result obtained above should be considered only as a qualitative estimate of a possible orbital symmetries in the ground state of ^{14}O nucleus for the $p^{13}\text{N}$ channel.

We now consider the basic characteristics of ^{14}O nucleus, which has in the GS $J^\pi = 0^+$ the energy 4.628 MeV [27]. Since for the ^{13}N nucleus $J^\pi = 1/2^-$ [27], the GS of ^{14}O in the $p^{13}\text{N}$ channel can be associated with the 3P_0 state. Below this threshold, there are no bound excited states (ES) [27]. Above the threshold, there are the following resonance states (RS):

1. For the first resonance, which plays the most important role in determining the magnitude of the astrophysical S -factor, the new data [17] lead to an excitation energy of 5.164(12) MeV (here and below numbers in parentheses are uncertainties), which corresponds to the energy $E_{res} = 536(12)$ keV relative to the threshold in the center-of-mass (c.m.), the width $\Gamma_{res} = 38(2)$ keV, and moment $J^\pi = 1^-$. Previously in Ref. [28] it was reported for this level the excitation energy of 5.156(2) MeV, i.e. $E_{res} = 0.528(2)$ MeV and the width $\Gamma_{res} = 37.3(9)$ keV. In an earlier work [27], for this resonance was reported the excitation energy 5.173(10) MeV, i.e. $E_{res} = 545(10)$ keV and the width $\Gamma_{res} = 38.1(1.8)$ keV. In fact, these three results lead to the same 38(2) keV widths. However, the resonance energies do not overlap within the experimental errors and can be in the range of $E_{res} = 524 - 555$ keV. This resonance can be matched to the 3S_1 or 3D_1 states, and $E1$ transitions $^3S_1 \rightarrow ^3P_0$ or $^3D_1 \rightarrow ^3P_0$ are possible. In this paper, we assume that such a state is a 3S_1 wave.

All other resonances, as can be seen below, do not make a significant contribution to the S -factor at low energies, and their energies, as follows from Refs. from [17] and [28], practically overlap. Therefore we use the data [28], but for a comparison we also give the energies and widths obtained in Ref. [17].

2. At an excitation energy of 5.710(20) MeV or 1.082(20) MeV relative to the channel's threshold in the c.m., there is a state $J^\pi = 0^-$ with a width of 400(45) keV [28], which can be associated with a 1S_0 wave. However, in this case, the transition to the GS is impossible, because it refers to a triplet state.

3. At an excitation energy of 5.920(10) MeV, i.e. $E_{res} = 1.29(10)$ MeV, there is a state $J^\pi = 0^+$ with a width $\Gamma_{res} < 12$ keV [17], which can be matched to a 3P_0 wave. In Ref. [17] the energy 5.931(10) MeV and the width less than 12 keV were reported. From this wave, magnetic transitions to the GS are impossible.

4. At an excitation energy of 6.284(9) MeV [$E_{res} = 1.656(9)$ MeV in the c.m.], there is a state $J^\pi = 3^-$ with the width $\Gamma_{res} = 25(3)$ keV [28], while in Ref. [17] the energy 6.285(12) MeV and the width 38(17) keV are obtained. This state can be matched to a F_3 wave. From this wave, only the $M3$ transition is possible, which is omitted in our consideration.

5. At an excitation energy of 6.609(10) MeV [$E_{res} = 1.981(10)$ MeV], there is a state $J^\pi = 2^+$ with a width $\Gamma_{res} < 5$ keV [28], which can only be associated with a 3P_2 or 3F_2 waves. In Ref. [17] the energy 6.585(11) MeV and the width less than 25 keV is reported. For 3F_2 wave the $E2$ transition is possible and we evaluate its effect.

6. At an excitation energy of 6.767(11) MeV [$E_{res} = 2.139(11)$ MeV], there is a state $J^\pi = 2^-$ with the width $\Gamma_{res} < 90(5)$ keV [28]. Based on the results [17], the energy is 6.764(10) MeV and the width is 96(5) keV. This state can be associated with a 3D_2 wave. From this wave, only $M2$ transition to the GS is possible. This transition is omitted, because we restrict ourself with the consideration of the $M1$ transition only.

7. At an excitation energy of 7.768(10) MeV [3.140(10) MeV in the c.m.] for the state $J^\pi = 2^+$ the width of 68(6) keV was observed in Ref. [17], while Ref. [28] reported 7.745(19) MeV [$E_{res} = 3.117(19)$] and 62(10) keV for the energy and the width, respectively. This resonance state can be associated with the 3P_2 or 3F_2 waves. From the 3F_2 wave the $E2$ transition to the GS is possible and we evaluate its effect.

8. Recently, in Ref. [17] at the excitation energy of 9.755(10) MeV or 5.123(11) MeV relative to the threshold of the $p^{13}\text{N}$ channel, a state $J^\pi = 2^+$ with the width $\Gamma_{res} = 229(51)$ keV was observed. While the excitation energy is in good agreement with the results from Ref. [28], 9.751(11) MeV, the width of the resonance is almost twice bigger. Moreover, a moment $J^\pi = 2^+$ of this state was in question in [28], but in the recent work [17] it was finally determined. This state can also be associated with 3P_2 or 3F_2 waves. From the 3F_2 wave the $E2$ transition to the GS is also possible, and we will take into account its effect.

As a result of the analysis of the above mentioned resonances, it turns out that, first of all, it is necessary to consider the $E1$ transition from the first resonance at $E_{res} = 0.536(12)$ MeV with $J^\pi = 1^-$ and the width $\Gamma_{res} = 38(2)$ keV [17]. In addition, we consider two other values for the energy of this resonance $E_{res} = 528(2)$ keV with the width $\Gamma_{res} = 37.3(9)$ keV [28] and $E_{res} = 545(10)$ keV with the width $\Gamma_{res} = 38.1(1.8)$ [27]. In addition to the $E1$ transition, there are three $E2$ transitions for $J^\pi = 2^+$, $E_{res} = 1.981(10)$ MeV, $\Gamma_{res} = 5$ keV, $J^\pi = 2^+$, $E_{res} = 3.140(10)$ MeV, $\Gamma_{res} = 68(6)$ keV, and $J^\pi = 2^+$, $E_{res} = 5.123(11)$ MeV, $\Gamma_{res} = 229(51)$ keV resonance states, which are admissible and can be associated with 3F_2 wave. We also consider the $M1$ transition for the $J^\pi = 0^+$, $E_{res} = 1.29(10)$ MeV of a non-resonance 3P_1 scattering wave to the GS of ${}^{14}\text{O}$. Resonances with higher energies either have a large moment, or their moment is not determined at all [28] and are not considered here.

IV. INTERACTION POTENTIALS

To find the radial wave functions χ_i and χ_f of relative motion of particles in the initial and final states, one should solve the Schrödinger equation with potentials that describe the $p^{13}\text{N}$ scattering process and the states of the residual ${}^{14}\text{O}$ nucleus. The $p^{13}\text{N}$ potentials for each partial wave, i.e., for the given orbital angular momentum L have a point-like Coulomb term, and a nuclear part of the $p^{13}\text{N}$ interaction. The nuclear part of potential can be written in the one-range Gaussian form as [29, 32]

$$V(r, SLJ) = -V_0(SLJ) \exp(-\alpha_{SLJ} r^2), \quad (9)$$

where r is the distance between the proton and ${}^{13}\text{N}$, $V_0(SLJ)$ is the depth of the potential and α_{SLJ} is the range parameter for given S , L , and J , respectively. Resonance potentials were constructed in such a way as to correctly describe the energy and width of such resonances. In calculations we use for the proton mass $m_p = 1.007276469$ amu [40] and ${}^{13}\text{N}$ mass 13.0057367 amu [41], where 1 amu = 931.4941024 MeV [40] and the constant $\hbar^2/m_0 = 41.4686$ MeV \cdot fm 2 . The Coulomb potential at $R_C = 0$ is written in MeV as $V_C(r) = 1.439975 Z_1 Z_2 / r$, where r is the interparticle distance in fm, Z_1 and Z_2 are charges of the particles in units of the elementary charge. The Sommerfeld parameter

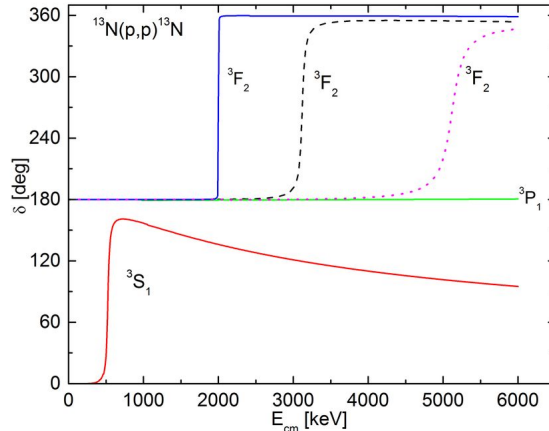


FIG. 1: (Color online) The dependence of the elastic $p^{13}\text{N}$ scattering phases on the energy. Calculations are performed using the potentials with parameters from Table I. The ${}^3\text{S}_1$ phase is calculated using the set 1c Table I.

$\eta = \mu Z_1 Z_2 e^2 / (k \hbar^2) = 3.44476 \cdot 10^{-2} \mu Z_1 Z_2 / k$, where $k = (2\mu E / \hbar^2)^{1/2}$ is the wave number specified in fm^{-1} and defined by the energy E of interacting particles, and the reduced mass μ of these particles in amu. In Table I are given the results of calculations of parameters for the corresponding potentials.

Following Ref. [42] for calculations of the width employing the resonance scattering phase we use the expression $\Gamma_{res} = 2(d\delta/dE)^{-1}$, where δ is the phase. In Fig. 1 the dependence of the elastic $p^{13}\text{N}$ scattering phases on the energy E_{cm} . The result of calculation of the ${}^3\text{S}_1$ phase with the set 1c parameters for the S scattering potential without FS lead to $90^\circ \pm 1^\circ$ at the energy $E_{res} = 0.545$ MeV are presented. The result is shown by the red solid curve. For the ${}^3\text{P}_1$ scattering potential, one can use the parameter set 2 from Table I. Such a potential has the FS and leads to scattering phases of $180^\circ \pm 1^\circ$ and is presented by the green solid curve in the energy range from zero to 7 MeV. Since it has the FS, according to the generalized Levinson theorem, its phase begins at 180° [37].

We also considered the $J^\pi = 2^+$, $E_{res} = 1.981(10)$ MeV, $\Gamma_{res} = 5$ keV, $J^\pi = 2^+$, $E_{res} = 3.140(10)$ MeV, $\Gamma_{res} = 68(6)$ keV, and $J^\pi = 2^+$, $E_{res} = 5.123(11)$ MeV, $\Gamma_{res} = 229(51)$ keV resonances, which lead to a noticeable change in the S -factor in resonance regions using the potentials with the parameters set 3, 4 and 5, respectively, from Table I. However, it was not possible to construct such potentials in P -waves, therefore, F scattering waves were

TABLE I: List of transitions from the initial $\left\{ \begin{matrix} (2S+1) \\ L_f \end{matrix} \right\}_i$ state to ${}^3\text{P}_0$ GS of ${}^{14}\text{O}$ nucleus. The value of P^2 determines the coefficient in expressions (3) and (6). The width Γ_{res} and $S(0)$ -factor are obtained using the potential parameters V_0 and α . The value $\tilde{S}(0)$ of the S -factor and the set of parameters 1d, 1e, and 1f for the potential are used for calculations of the resonance width $\tilde{\Gamma}_{res}$.

Set	$\left\{ \begin{matrix} (2S+1) \\ L_f \end{matrix} \right\}_i$	Transition	P^2	V_0 , MeV	α , fm^{-2}	E_{res} , MeV	Γ_{res} , keV	$S(0)$, keV·b	$\tilde{\Gamma}_{res}$, keV	$\tilde{S}(0)$, keV·b	
1	${}^3\text{S}_1$ resonance at 0.528, 0.536, 0.545 MeV	$E1$	1	a	14.955	0.085	0.528(1)	37(1)	8.4(2)		
				b	15.882	0.092	0.536(1)	38(1)	7.9(2)		
				c	18.244	0.11	0.545(1)	37(1)	7.0(2)		
				d	35.053	0.25	0.528(1)			22(1)	4.8(1)
				e	29.316	0.02	0.536(1)			25(1)	5.1(1)
				f	31.582	0.22	0.545(1)			26(1)	4.9(1)
2	${}^3\text{P}_1$ no resonance	$M1$	2	555.0	1.0			0.014(1)			
3	${}^3\text{F}_2$ resonance at 1.981(10)	$E2$	3	698.134	0.36	2.000	13	< 0.01			
4	${}^3\text{F}_2$ resonance at 3.117(19)	$E2$	3	343.613	0.18	3.120	58	< 0.01			
5	${}^3\text{F}_2$ resonance at 5.123(11)	$E2$	3	430.2	0.23	5.127	232	< 0.01			

used here. The first of them leads to a resonance at 2.00 MeV with a width $\Gamma_{res} = 13$ keV shown by the blue solid curve in Fig. 1, the second gives the resonance at $E_{res} = 3.12$ MeV and a width $\Gamma_{res} = 58$ keV and is presented by the black dashed curve, while the phase of the third resonance at $E_{res} = 5.127$ MeV is shown by the dotted curve. We were not able to obtain the resonance at $E_{res} = 1.981$ MeV with the width $\Gamma_{res} < 5$ keV, as given in [28], but the obtained value is completely consistent with the recent data [17].

To build the potential for description of the GS of ^{14}O , we use the experimental binding energy and the asymptotic normalization coefficient (ANC) of this state. The corresponding potentials are tested based on the calculation of the root mean square charge radius of ^{14}O .

In Ref. [15] the value of $ANC = 5.42(48)$ fm $^{-1/2}$ and the proton spectroscopic factor $S_p = 1.88(34)$ are given. A similar value of $ANC = 5.42(74)$ fm $^{-1/2}$ is also reported in Ref. [16], while Ref. [22] reports $ANC = 5.39(38)$ fm $^{-1/2}$. Using the results of [15] for the ANC and the expression for the asymptotic normalization constant

$$ANC = \sqrt{S_p}C \quad (10)$$

one gets $C = 4.04(72)$ fm $^{-1/2}$. For determination of C , the following definition is also used (see, for example, [46])

$$\chi_L(r) = CW_{-\eta, L+1/2}(2k_0r), \quad (11)$$

where $W_{-\eta, L+1/2}(2k_0r)$ is a Whittaker function. We use a different definition of ANC [47]

$$\chi_L(r) = \sqrt{2k_0}C_w W_{-\eta, L+1/2}(2k_0r) \quad (12)$$

which differs from the previous definition by the factor $\sqrt{2k_0}$ that is in this case 0.956. Then for the dimensionless C_w we get $C_w = 4.23(75)$. At the same time in Ref. [22] $S_p = 0.90(23)$ was given for the spectroscopic factor, which yields $ANC = 5.39(38)$ fm $^{-1/2}$ and allows to obtain $C_w = 6.15(1.22)$. $ANC = 30.4(7.1)$ fm $^{-1}$ and $S_p = 1.94(45)$, were obtained in Ref. [23], which lead to the dimensionless asymptotic normalization constant within the range 3.26 – 5.30 with an average of 4.28(1.02).

The potential of a bound ground 3P_0 state with the FS should correctly reproduce the GS energy -4.628 MeV of ^{14}O nucleus with $J^\pi = 0^+$ in the $p^{13}\text{N}$ channel [27] and it is reasonable to describe the mean square radius of ^{14}O as well. Since data on the radius of ^{14}O are not available, we consider it to coincide with the radius of ^{14}N , the experimental value of which is 2.5582(70) fm [41]. As a result, we obtained the following parameters for the GS potential, which lead to $C_w = 4.1(1)$:

$$V_0(1, 1, 0^+) = 226.230 \text{ MeV}, \alpha(1, 1, 0^+) = 0.23 \text{ fm}^{-2}. \quad (13)$$

The potential (9) with the parameters (13) gives for the ^{14}O nucleus the binding energy of 4.628 MeV and the root mean square charge radius $R_{ch} = 2.55$ fm. We used 0.8768(69) fm for the proton radius [40] and 2.4614(34) fm for the ^{13}N radius. The latter radius was taken to be the radius of ^{13}C [41], because the ^{13}N radius is not available.

The GS potential which leads to $C_w = 6.1(1)$ has parameters

$$V_0(1, 1, 0^+) = 156.728 \text{ MeV}, \alpha(1, 1, 0^+) = 0.15 \text{ fm}^{-2}. \quad (14)$$

The GS potential with parameters (14) gives a binding energy of 4.628 MeV and the root mean square charge radius $R_{ch} = 2.63$ fm.

We use the potentials with parameters from sets 1a, 1b and 1c in Table I for the description of the resonance states and parameters (13) and (14) for the description of the residual ^{14}O nucleus for calculations of the $^{13}\text{N}(p, \gamma)^{14}\text{O}$ reaction rate and the astrophysical S -factor.

The astrophysical S -factor was calculated previously using the 3S_1 resonance scattering. Using the values of $\tilde{S}(0)$ from Table I, we consider the inverse problem to construct potentials for description the 3S_1 resonance based on the resonance energies and the corresponding astrophysical S -factor. The parameters of these potentials are given in Table I as sets 1d, 1e, and 1f.

V. REACTION RATE AND ASTROPHYSICAL S -FACTOR OF THE PROTON RADIATIVE CAPTURE ON ^{13}N

Let us calculate the reaction rate for the $^{13}\text{N}(p, \gamma)^{14}\text{O}$ radiative capture and the astrophysical S -factor using the total cross section (2) and corresponding matrix elements of multipole transition operators. The astrophysical factor $S(E)$ is defined as

$$S(E) = E\sigma_c(NJ, J_f)e^{-2\pi\eta}, \quad (15)$$

where the factor $\exp(-2\pi\eta)$ approximates the Coulomb barrier between two point-like particles with charges Z_1 and Z_2 and orbital momentum $l = 0$, while for the reaction rate is commonly expressed in $\text{cm}^3\text{mol}^{-1}\text{s}^{-1}$ and is determined according to Ref. [25] as

$$N_A \langle \sigma_c v \rangle = 3.7313 \times 10^4 \mu^{-1/2} T_9^{-3/2} \int_0^\infty \sigma_c(E) E \exp(-11.605E/T_9) dE, \quad (16)$$

where N_A is Avogadro's number, E is the energy in the center-of-mass frame given in MeV, the cross section $\sigma_c(E)$ is measured in μb , μ is the reduced mass in a.m.u, and T_9 is the temperature in units of 10^9 K. The behavior of S -factor, when resonances are present, in general, is expected to be rather smooth at low energies and can be expanded in Taylor series around $E = 0$ [48, 49]. Retaining only the first three terms of the Taylor series and ignoring higher-order terms, one obtains

$$S(E) = S_0 + ES_1 + E^2S_2. \quad (17)$$

The expression (17) is the well known approximation for the S -factor at low energies range of 30–200 keV.

Essentially, the experimental data on the astrophysical S -factor of the proton radiative capture on ^{13}N are absent, but in the database [50] there are rates of this reaction from Refs. [7, 15]. However, it is clear that the shape of S -factor should mainly be determined by resonance in the 3S_1 scattering wave at 0.528 MeV with a width $\Gamma_{res} = 37.3(9)$ keV and $J^\pi = 1^-$ [28]. The contributions of cross sections of 3F_2 resonances from Table I, which are determined by $E2$ transitions, are possible as well.

For calculations of the astrophysical S -factor we use the potentials with parameters from sets 1a, 1b and 1c in Table I for the description of the resonance state and parameters (13) and (14) for the description of the residual ^{14}O nucleus. We also calculate the width of 3S_1 resonance using the sets of the parameters 1d, 1e and 1f for the potentials from Table I, which were obtained based on the values of the astrophysical S -factor.

The results of calculating S -factor of the radiative proton capture on ^{13}N to the GS of ^{14}O nucleus from 3S_1 scattering wave with the set of parameters 1a in Table I for the potential and potential (13) for the GS are shown in Fig. 2. We calculated the contributions of the $M1$ transition $^3P_1 \rightarrow ^3P_0$, as well as the resonant $E2$ transitions into the S -factor using the set of the potentials 2, 3, 4, and 5 from Table I, respectively, and for the description of the GS the potential (13) was used. The results of these calculations are shown in Fig. 2. Analysis of results presented in Fig. 2 shows that contributions of the $M1$ and $E2$ transitions in the S -factor are negligible at energies $E < 1$ MeV, but are significant at high energies. At the resonance energy, the S -factor reaches 2.4 MeV·b, which is in good agreement with the results of other works (see, for example, Refs. [7, 15, 18, 22]), where the values for the S -factor from about 2.0 to 2.5 keV·b were reported. Results of our calculations for the S -factor for the potentials 1a from Tables 1 and (13) in the energy range of 30 – 50 keV lie in the range of 8.2 – 8.3 keV·b, while in the energy range of 30–70 keV, the average value is 8.4(2) keV·b. The error given here is determined by averaging S -factor over the above energy range. Known results for the S -factor at zero energy lead to a value in the range from 2.0 keV·b to 6.0 keV·b [7, 15, 18, 22]. We use the GS potential (14) and calculate the S -factor in the energy range 30 – 70 keV using the set of parameters 1a from Table I for the potential and obtain almost constant value $S = 11.9(2)$ keV·b. At the resonance energy the S -factor reaches 2.9 MeV·b, which is noticeably more than the results of [7, 15, 18, 22]. Therefore, we should mention that the GS potential with the parameters (13) for description of the GS of ^{14}O nucleus in the $p^{13}\text{N}$ channel at low energy region leads to more preferable results for the astrophysical S -factor, which are quite consistent with results from previous calculations. Our calculations for the S -factor with the parameters (14) for the potential of the GS gives too high value for the S -factor at low energies. However, since there are no experimental measurements of the S -factor for this reaction, no final conclusions can be drawn.

Table II gives the compilation of the results for the astrophysical S -factors at zero energy obtained in different works. As it can be seen from Table II, the deviation of data for the S -factor is in the range from 2 to 6 keV·b, although the most recent value is apparently given in Ref. [26]. We use the sets of parameters 1a, 1b, and 1c for the potential of 3S_1 scattering from Table I and potential (13) for the GS, which reproduce accurately the position and width of resonances and calculated corresponding S -factors. The results are presented in Table I. Depending on the resonance energy S -factors are: 8.4(2) keV·b ($E_{res} = 528(1)$ keV), 7.9(2) keV·b ($E_{res} = 536(1)$ keV), and 7.0 keV·b ($E_{res} = 545(1)$ keV). The potential with the set 1a from Table I accurately reproduces the width average value of 37 keV [28] and leads to $S(0) = 8.4(2)$ keV·b. The potential with the set 1b reproduces the resonance energy of 536(12)

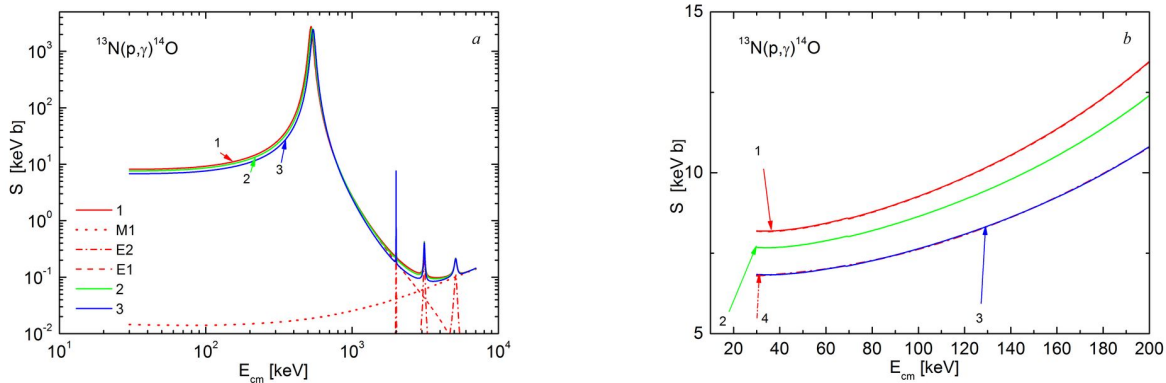


FIG. 2: (Color online) Astrophysical S -factor of the radiative proton capture on ^{13}N in the energy range (a) 30 keV – 7 MeV. The solid curve 1 presents results of calculations of the $E1$ transition for the potentials with the set of parameters 1a from Table (I) and GS (13). The dashed and dotted curves represent the results for $E2$ and $M1$ transitions, respectively, obtained with the set of parameters 2, and 3–5 from Table I and GS (13). The solid curves 2, and 3 – are results of calculations with the set of parameters 1b and 1c from Table I, respectively, and GS (13); (b) 30 – 200 keV. The solid curves 1, 2, and 3 presents results for potentials with the set of parameters 1a, 1b, and 1c from Table I, respectively, and GS (13). The dash-dotted curve 4, which coincides with the curve 3, presents the quadratic approximations (17) of the S -factor at low energies.

keV and the width $\Gamma_{res} = 38(2)$ keV from Ref. [17]. The corresponding average value for the S -factor at 30–70 keV is $S(0) = 7.9(2)$ keV·b, which is slightly less than for the S scattering potential 1a. We consider a potential with parameters 1c, which leads to the resonance at 545 keV and a width $\Gamma_{res} = 37(1)$ keV [27]. This potential gives $S(0) = 7.0(2)$ keV·b.

Nevertheless, let us try to find out whether it is possible within our approach to obtain the S -factor at zero energy that is close to the results of [26], namely, $3.8^{+1}_{-0.8}$ keV·b. We constructed S -wave scattering potentials, which with the potential (13) for the GS, allow us to obtain maximum value of the S -factor about 4.8 – 5.0 keV·b given in Ref. [26]. Such potentials have the set of parameters 1d, 1e, and 1f listed in Table I. These potentials lead to the resonance energies 528(1) keV, 536(1) keV, and 545(1) keV, respectively, but the corresponding widths are significantly smaller than reported in Refs. [17, 27, 28]. In particular, the set 1d leads to $E_{res} = 528(1)$ keV, but the width is $\tilde{\Gamma}_{res} = 22(2)$ keV. At 30 keV $\tilde{S}(0) = 4.8$ keV·b and its average value in the range of 30 – 70 keV is $\tilde{S}(0) = 4.8(1)$ keV·b. If for the potential with a resonance energy of 536 keV, we use the parameters 1e from Table I, which lead to $\tilde{\Gamma}_{res} = 25(1)$ keV, then the S -factor decreases to $\tilde{S}(0) = 5.1(1)$ keV·b. The S -factor decreases to $\tilde{S}(0) = 4.9(1)$ keV·b, when we use the set 1f for the potential and the width becomes $\tilde{\Gamma}_{res} = 26(1)$ keV. Thus, in principle, all previously obtained results for the S -factor at zero energy can be reproduced, but the width of the resonances does not correspond to the data [17, 27, 28]. Therefore, for the considered resonance energies, if we correctly describe their widths, makes impossible to obtain the S -factor below 7.0 (2) keV·b. Only a decrease in the resonance width to 25–26 keV with its energy of 536–545 keV leads to the S -factor of the order of 4.9–5.1 keV·b.

We use Eq. (17) for the approximation of the S -factor at low energies. The corresponding parameters are: $S_0 = 6.7645 \times 10^{-2}$, $S_1 = -2.7612 \times 10^{-3}$, $S_2 = 1.1428 \times 10^{-4}$ at $\chi^2 = 1.0 \times 10^{-3}$. The results are shown in Fig. 2b by the dash-dotted curve 4 that coincides with the curve 3, which presents the results of calculations for the potentials

TABLE II: Astrophysical S -factors at zero energy.

Refs.	[26]	[15, 16, 18, 22, 23] ^a	[20] ^b	[27] ^a
S , keV·b	$3.8^{+1}_{-0.8}$	5 – 6	2.6	2 – 2.3

^aValues are taken from Figures in Refs: [16] – Fig. 7; [17] – Fig. 8; [18] – Fig. 9; [23] – Fig. 5; [25] – Fig. 3; [27] – Fig. 2b.

^bValue is taken from the approximation at low energies.

TABLE III: The results of the dependence of the $p^{13}\text{N}$ reaction rate on temperature.

Temperature, T_9	Reaction rate, $\text{cm}^3\text{mol}^{-1}\text{s}^{-1}$	Temperature, T_9	Reaction rate, $\text{cm}^3\text{mol}^{-1}\text{s}^{-1}$
0.01	4.81E-22	0.35	2.53E-01
0.02	6.46E-16	0.4	9.10E-01
0.03	5.94E-13	0.45	2.91E+00
0.04	4.37E-11	0.5	8.04E+00
0.05	9.28E-10	0.6	4.02E+01
0.06	9.54E-09	0.7	1.30E+02
0.07	6.14E-08	0.8	3.13E+02
0.08	2.86E-07	0.9	6.13E+02
0.09	1.05E-06	1	1.04E+03
0.1	3.22E-06	1.5	4.53E+02
0.11	8.61E-06	2	8.46E+03
0.12	2.06E-05	2.5	1.15E+04
0.13	4.49E-5	3	1.35E+04
0.14	9.09E-05	3.5	1.46E+04
0.15	1.73E-04	4	1.51E+04
0.16	3.12E-04	4.5	1.52E+04
0.17	5.37E-04	5	1.51E+04
0.18	8.90E-04	6	1.44E+04
0.19	1.42E-03	7	1.35E+04
0.2	2.21E-03	8	1.25E+04
0.25	1.40E-02	9	1.16E+04
0.3	6.46E-02	10	1.08E+04

TABLE IV: Parameters of the analytical parametrization of the $^{13}\text{N}(p, \gamma)^{14}\text{O}$ reaction rate for the present calculations based on Eq. (18) and NACRE II data [26] based on Eq. (18) as well.

Parameters	a_1	a_2	a_3	a_4	a_5	a_6	a_7
Present work, Eq. (18)	4.68425	5.5271	72207.8	-2.86832	-17716.6	-1304.726	-1155.274
NACRE II	77.14845	4.87776	-2791.957	7554.465	-4686.978	3691.79	-4033.686
Parameters	a_8	a_9	a_{10}	a_{11}	a_{12}	a_{13}	a_{14}
Present work, Eq. (18)	-1020.536	215.4007	4.66187×10^6	10.92388	8.5529×10^7	15.50687	16674.76
NACRE II	1901.048	-309.4704	-3320.309	7.12181	3.13709×10^8	15.87507	-13.31191
Parameters	a_{15}		a_{16}		a_{17}		
Present work, Eq. (18)	7.86955		-77.74082		1.38331		
NACRE II	5.65906		-48.07274		1.23332		

with the set of parameters 1c from Table I and GS (13).

Using Eq. (16), we calculated the rate of the $^{13}\text{N}(p, \gamma)^{14}\text{O}$ radiative capture. The dependence of the $^{13}\text{N}(p, \gamma)^{14}\text{O}$ reaction rate on astrophysical temperature is shown in Fig. 3. The corresponding rates are tabulated in Table IV for $0.01 < T_9 < 10$. The calculations are performed using the set of parameters 1a and (13) for the potentials. Let us mention that the earlier calculations [15, 18, 22] practically coincide with our results, while results from Ref. [7] at temperatures $T_9 > 1$ are up to 2 times lower than present results. The results of calculations with the set of parameters 1a and (14) for the potentials give a noticeable excess of the reaction rate over the rates obtained with the GS potential (13) at temperatures above 1 T_9 .

Following Ref. [51] the reaction rate obtained in our calculations is parameterized as

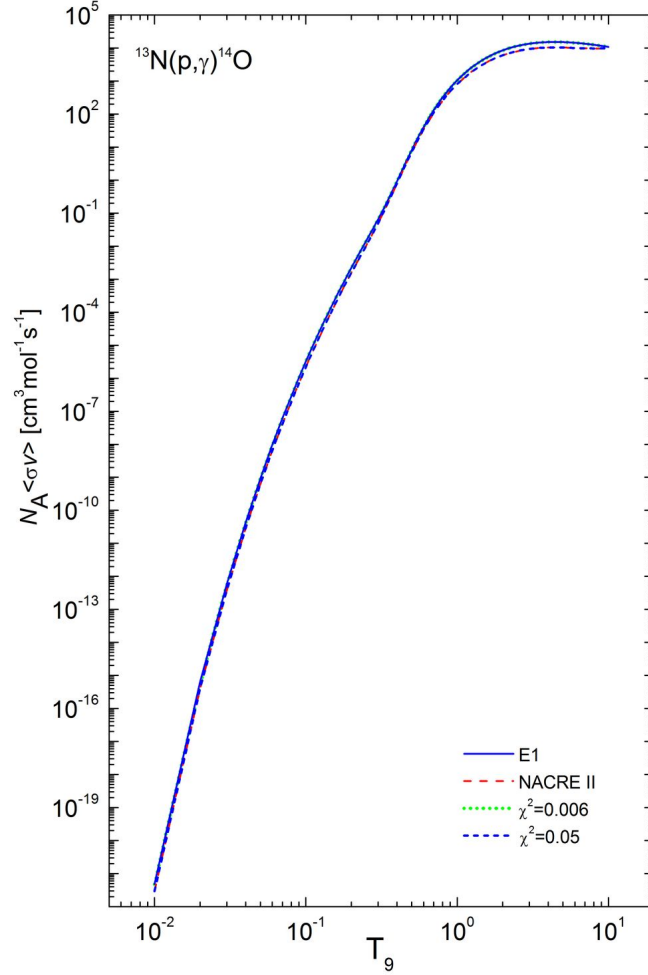


FIG. 3: (Color online) The dependence of the reaction rate of $p^{13}N$ radiative capture on astrophysical temperature for the $E1$ transition. Calculations performed for the potentials with the set of parameters 1a from Table (I) and GS (13). The NACRE II data [26] are presented using Eq. (18) with parameters from Table IV.

$$N_A \langle\sigma v\rangle = \frac{a_1}{T} \exp\left(-\frac{a_2}{T}\right) \left(1 + a_3 T^{1/3} + a_4 T^{2/3} + a_5 T^{4/3} + a_7 T^{5/3} + a_8 T^{6/3} + a_9 T^{7/3}\right) + \frac{a_{10}}{T^{1/2}} \exp\left(-\frac{a_{11}}{T^{1/2}}\right) + \frac{a_{12}}{T} \exp\left(-\frac{a_{13}}{T^{1/3}}\right) + \frac{a_{14}}{T^{1/3}} \exp\left(-\frac{a_{15}}{T^{1/2}}\right) + \frac{a_{16}}{T^2} \exp\left(-\frac{a_{17}}{T^2}\right). \quad (18)$$

For the approximation 1000 calculated points of the reaction rate were used. The value T denotes T_9 , and the error for reaction rate for calculating χ^2 was set at the level of 5%. The parameters for the reaction rate (18) from Table III lead to $\chi^2 = 0.006$, and allow to merge with the calculated reaction rate using Eq. (18). Results of calculations using Eq. (18) are presented in Fig. 3 by the dotted curve. It almost merges with a blue solid curve that shows the calculated reaction rate using Eq. (16) that is given in Table III. We parametrized the NACRE II data [26] using the same Eq. (18) with $\chi^2 = 0.05$ and 5% errors, which leads to the parameters listed in Table IV. The corresponding results of calculations are shown in Fig. 3 by the dashed curve.

For the comparison of the dependence of the reaction rate on astrophysical temperature, we calculated the ratio of our reaction rate to the rates from Refs. [15, 18, 22, 23, 26]. The results of this comparison are shown in Fig. 4a. It can be seen from Fig. 4a that the results of present calculations exceed NACRE II up to 1.7 times at the lowest temperatures and are almost equal to them at a temperature of $10 T_9$. The results of other studies lead to values that go below present calculations up to 1.2 times at a temperature of $0.01 T_9$, and in the range of $0.4 - 0.5 T_9$ practically coincide with our data. But as the temperature tends to $1 T_9$, the values again become less than ours by 1.2 times. In Fig. 4b are presented the ratios of the reaction rates obtained in the present work and in Refs. [15, 18, 22, 23] to the NACRE II [26] which is parameterized with the parameters from Table III.

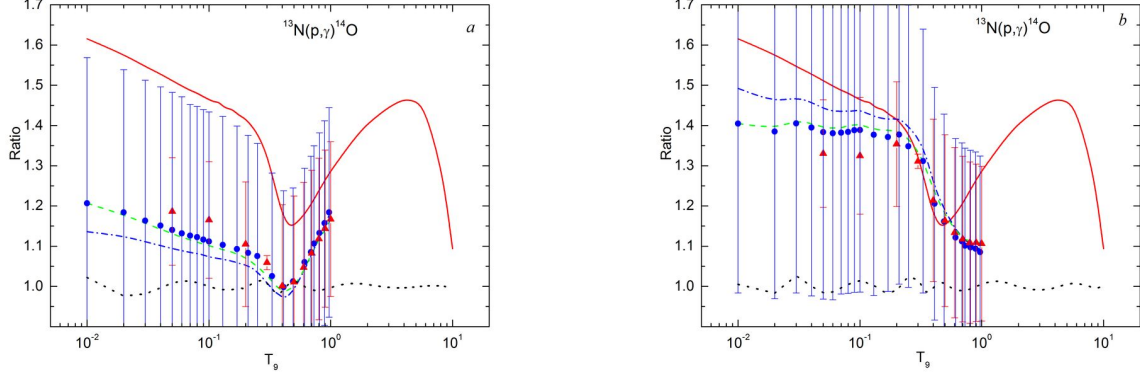
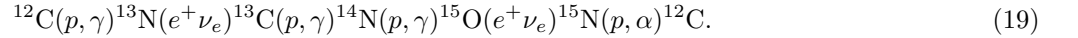


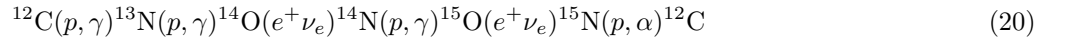
FIG. 4: (Color online) The dependence of the ratio of the reaction rates on temperature. (a) The ratio of the reaction rate obtained in the present calculations and given in Refs. [15, 18, 22, 23, 26], correspondingly : NACRE II [26] - solid curve, Li, et al. [15] - dash-dotted curve, Guo, et al. [19] - dashed curve, Tang, et al. [22] - circles with error bars, Magnus, et al. [18] - triangles with error bars, the dotted curve is the ratio of the estimated speed to its approximation (18); (b) The ratio of the reaction rates obtained in the present calculations, Refs. [15, 18, 22, 23] to the NACRE II [26] approximated with parameters from Table IV: present calculations - solid curve, Li, et al. [15] - dashed curve, Guo, et al. [19] - dash-dotted curve, Tang, et al. [22] - circles with error bars, Magnus, et al. [18] - triangles with error bars, correspondingly. The dotted curve corresponds to the ratio of NACRE II data and its approximation using the parameters from Table IV.

VI. CNO AND HOT CNO CYCLES

Since the late 1930s, when von Weizsäcker [52] and Bethe [53] independently proposed sets of fusion reactions by which stars convert hydrogen to helium, it is well established that the carbon-nitrogen-oxygen cycles is a mechanism for hydrogen burning in stars. The dominant sequence of reactions for this cycle is the following



The character of the nuclear burning is extremely temperature sensitive and, when temperatures is low enough, the hot carbon-nitrogen-oxygen cycle



starts. Since, at low T_9 temperatures the $^{13}\text{N}(p, \gamma)^{14}\text{O}$ reaction in the sequence (20) is competitive with the $^{13}\text{N}(e^+ \nu_e)^{13}\text{C}$ decay in the sequence (19), the formation and decay of ^{14}O becomes a major distinguishing feature of this higher temperature cycle. Therefore, the stellar $^{13}\text{N}(p, \gamma)^{14}\text{O}$ reaction rate determines the order and the precise temperature of the conversion of the cold CNO cycle to the HCNO cycle and the waiting point in the cycle changes from ^{14}N to the ^{14}O and ^{15}O and the $^{13}\text{N}(p, \gamma)^{14}\text{O}$ reaction is a key process which determines this conversion. Let's use our results for the $^{13}\text{N}(p, \gamma)^{14}\text{O}$ reaction rate, follow Ref. [11] and find the temperature window and densities of a stellar medium at which the CNO cycle is converted to the hot CNO cycle. We can achieve the latter by comparing the $^{13}\text{N}(p, \gamma)^{14}\text{O}$, $^{14}\text{N}(p, \gamma)^{15}\text{O}$ and $^{12}\text{C}(p, \gamma)^{13}\text{N}$ reaction rates and the lifetime of nuclei against destruction by hydrogen burning.

The lifetime of isotopes in the stellar CNO cycle relative to the combustion of hydrogen one can determine as follows [49, 54]

$$\tau = \frac{A_H}{\rho X_H} \frac{1}{N_A \langle \sigma_c v \rangle}, \quad (21)$$

where A_H is the atomic mass of hydrogen, X_H is the relative abundance of hydrogen by mass, ρ is the density of the stellar medium, and $N_A \langle \sigma_c v \rangle$ is the appropriate proton-capture reaction rate. Thus, as it is follows from Eq. (21), lifetime is determined precisely by the rate of the corresponding reaction. In our calculations we use the $^{12}\text{C}(p, \gamma)^{13}\text{N}$,

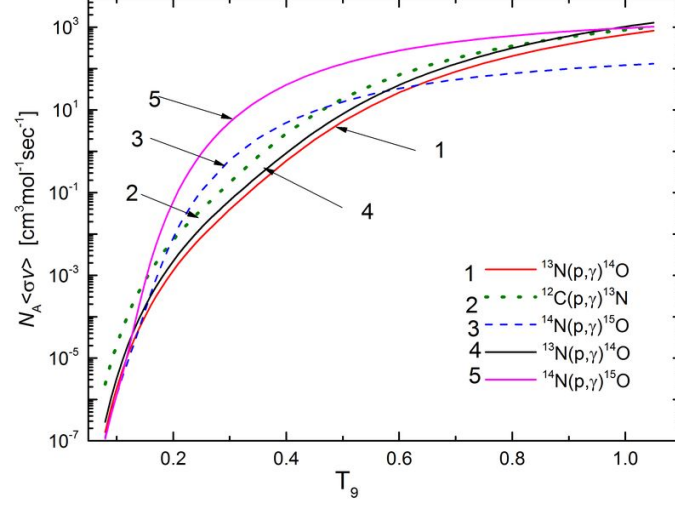


FIG. 5: (Color online) The dependence of the reaction rates $N_A \langle \sigma_c v \rangle$ on temperature for the $^{12}\text{C}(p, \gamma)^{13}\text{N}$, $^{13}\text{N}(p, \gamma)^{14}\text{O}$, and $^{14}\text{N}(p, \gamma)^{15}\text{O}$ reactions. Curves: 1, 2 and 3 - the data are taken from Ref. [11], 4 - present calculation, 5 - results from Ref. [34].

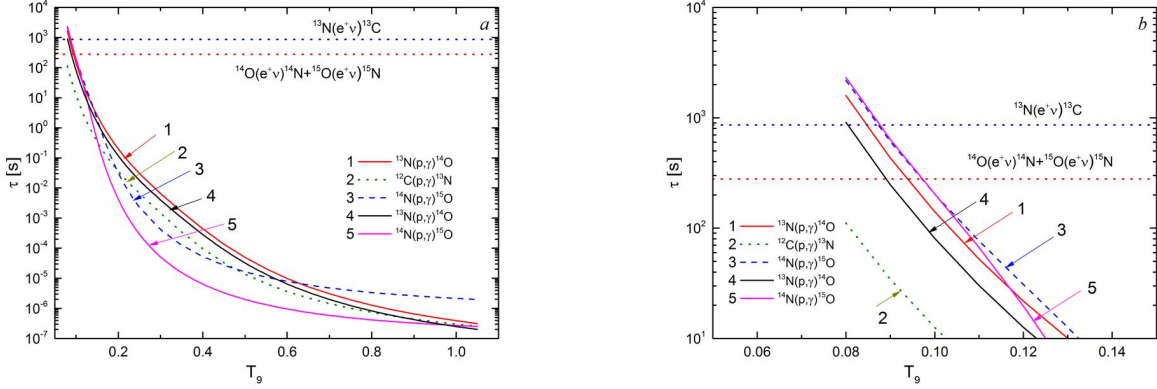


FIG. 6: (Color online) Comparison of lifetime against hydrogen burning via the $^{12}\text{C}(p, \gamma)^{13}\text{N}$, $^{13}\text{N}(p, \gamma)^{14}\text{O}$, and $^{14}\text{N}(p, \gamma)^{15}\text{O}$ reactions as a function of temperature, and the ^{13}N , ^{14}O , and ^{15}O β -decay rates for the temperature intervals $0.08 < T_9 < 1.0$ (a) and $0.08 < T_9 < 0.14$ (b).

$^{13}\text{N}(p, \gamma)^{14}\text{O}$, and $^{14}\text{N}(p, \gamma)^{15}\text{O}$ reactions rates. In Fig. 5 the reaction rates of the $^{13}\text{N}(p, \gamma)^{14}\text{O}$, $^{14}\text{N}(p, \gamma)^{15}\text{O}$ and $^{12}\text{C}(p, \gamma)^{13}\text{N}$ processes are shown, which are further used in the calculations of τ . For the $^{13}\text{N}(p, \gamma)^{14}\text{O}$ reaction we use results of the present calculations and data from Ref. [11], for the reaction $^{14}\text{N}(p, \gamma)^{15}\text{O}$ data [51] and [34] are used, while for the $^{12}\text{C}(p, \gamma)^{13}\text{N}$ we employed data [51], which are very close to data given in the NACRE II database [26]. Let us comment on the difference in the data for the $^{14}\text{N}(p, \gamma)^{15}\text{O}$ reaction (curves 3 and 5 in Fig. 5). In contrast to Ref. [51], in Ref. [34] the $^{14}\text{N}(p, \gamma)^{15}\text{O}$ reaction rate was calculated by taking into account radiative capture of protons both in the GS of ^{14}N nucleus and in all four excited bound levels. Such consideration allows to describe experimental data for the astrophysical S -factors of the radiative proton capture on ^{14}N to five excited states of the ^{15}O nucleus at the excitation energies of 5.18 MeV to 6.86 MeV under the assumption, that all five resonances are D scattering waves. The latter leads to the significant increase of the $^{14}\text{N}(p, \gamma)^{15}\text{O}$ reaction rate at temperatures $T_9 > 0.3$, which is indicated in Fig. 5.

In order to determine the astrophysical temperatures at which the CNO cycle is converted to the HCNO cycle, it is necessary to determine the $^{13}\text{N}(p, \gamma)^{14}\text{O}$ reaction rate as a function of temperature and compare it with one for the other processes. Using the reaction rates presented in Fig. 5, we calculate the dependence of the lifetime of isotopes produced in the processes $^{12}\text{C}(p, \gamma)^{13}\text{N}$, $^{13}\text{N}(p, \gamma)^{14}\text{O}$, and $^{14}\text{N}(p, \gamma)^{15}\text{O}$ on temperature. Following Ref. [11], in calculations we used for the hydrogen mass fraction $X_H = 0.77$ and the stellar density $\rho = 5 \times 10^3 \text{ g/cm}^3$ [55].

The dependencies of the lifetime of isotopes produced in the processes on the temperature are presented in Fig. 6. The data for the lifetime of radioactive isotopes are also presented in Fig. 6: $\tau_{^{13}\text{O}} = 863 \text{ s}$ for the $^{13}\text{N}(e^+\nu_e)^{13}\text{C}$, $\tau_{^{14}\text{N}} = 102 \text{ s}$ for the $^{14}\text{O}(e^+\nu_e)^{14}\text{N}$ and $\tau_{^{15}\text{N}} = 176 \text{ s}$ for the $^{15}\text{O}(e^+\nu_e)^{15}\text{N}$. The analysis of the results presented in Fig. 6 shows that at $T_9 = 0.08$ the $^{13}\text{N}(p, \gamma)^{14}\text{O}$ and $^{13}\text{N}(e^+\nu_e)^{13}\text{C}$ reactions have equal rates. When $^{13}\text{N}(p, \gamma)^{14}\text{O}$ reaction rate will exceed the $^{13}\text{N}(e^+\nu_e)^{13}\text{C}$ decay rate, the reaction sequence changes to the hot CNO cycle. For these conditions in CNO cycle the lifetimes of the β^+ -unstable systems such as ^{13}N and ^{15}O are long enough that proton capture can occur on these unstable nuclei before they undergo the β^+ -decay.

The onset of the HCNO cycle occurs at $T_9 = 0.08$ when the rate of the slowest $^{13}\text{N}(p, \gamma)^{14}\text{O}$ reaction exceeds the $^{14}\text{O}(e^+\nu_e)^{14}\text{N}$ and $^{15}\text{O}(e^+\nu_e)^{15}\text{N}$ decay rates. Moreover, at $T_9 = 0.1$ the ratio of the $^{13}\text{N}(p, \gamma)^{14}\text{O}$ and $^{13}\text{N}(e^+\nu_e)^{13}\text{C}$ rates is 10.8, in the contract to Ref. [11], where this ratio is about 6. Therefore, at $T_9 = 0.1$ the reaction $^{13}\text{N}(p, \gamma)^{14}\text{O}$ is already ten times faster than the $^{13}\text{N}(e^+\nu_e)^{13}\text{C}$ decay, resulting in the mass flow going via ^{14}O at the very onset of the HCNO cycle. The present result indicates that the HCNO cycle is turned on at the early stage of a nova explosion when the temperature is lower than reported in the earlier calculations [19] and [11].

Our calculations lead to the temperature range $0.13 < T_9 < 0.97$, where the reaction rate of $^{14}\text{N}(p, \gamma)^{15}\text{O}$ is greater than the reaction rate of $^{13}\text{N}(p, \gamma)^{14}\text{O}$. The $^{13}\text{N}(p, \gamma)^{14}\text{O}$ reaction rate obtained in the present calculations leads to the temperature window which is much wider than reported in Ref. [11]: $0.14 < T_9 < 0.64$. One should mentioned that the reaction rates for $^{13}\text{N}(p, \gamma)^{14}\text{O}$ in the present work and $^{14}\text{N}(p, \gamma)^{15}\text{O}$ [34] are obtained in the framework of the same theoretical approach.

Following Ref. [11], let's determine the dependence of the stellar medium density corresponding to the onset of the HCNO cycle on temperature as

$$\rho = \frac{A_H}{X_H(\tau_{^{14}\text{N}} + \tau_{^{15}\text{N}})} \frac{1}{N_A \langle \sigma_c v \rangle_{\min}}, \quad (22)$$

where the smallest reaction rate $N_A \langle \sigma_c v \rangle_{\min}$ includes the temperature dependence. An analysis of the density-temperature relationship allows to determine the temperatures and densities at which the stellar CNO cycle is con-

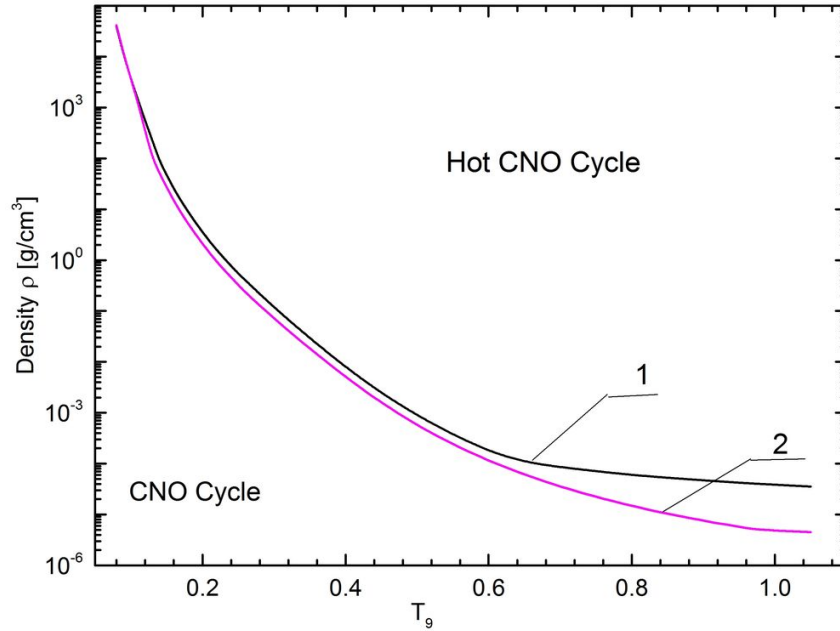


FIG. 7: (Color online) Density and temperature range for the operation of the hot CNO cycle. Curves: 1 - result from Ref. [11]; 2 - present result.

verted to the HCNO cycle. If the density and temperature of the stellar medium fall above the curve $\rho(T)$ on the density-temperature diagram, then HCNO cycle occurs, otherwise the CNO cycle operates.

The results of present calculations for the density-temperature dependence $\rho(T)$ along with results from Ref. [11] are shown in Fig. 7. The comparison of our calculations and results [11] indicates that at the same temperature range HCNO cycle operates at the lower densities of a stellar medium than in the case reported in [11]. Analyses of the results given at the density-temperature diagram in Fig. 7 demonstrate that at an early stage of a nova explosion at the temperature range $0.2 T_9 - 0.4 T_9$ the hot CNO cycle could be turned on at a twice less density of the stellar matter. The difference becomes more significant at $T_9 > 0.6$ and the HCNO cycle could be operated when at $1 T_9$ a stellar medium density becomes about 10 times less compared to [11], as can be seen from Fig. 7. Thus, in supermassive stars at high temperature the ignition of the hot CNO cycle can occur at much lower densities generating sufficient energy which can affect very massive stars collapse at the end of their life cycle.

VII. CONCLUSION

We briefly summarize our results. We have employed the modified potential cluster model to describe the $^{13}\text{N}(p, \gamma)^{14}\text{O}$ reaction at astrophysical energies and influence of the first $p^{13}\text{N}$ resonance width on the astrophysical S -factor. At energies of 30–70 keV, the S -factor remains almost constant with the average value 8.4(2) keV·b, thereby determining its value at zero energy, which is determined by the potential of the S -wave scattering. The potentials of the S -wave, leading to the correct resonance width for different resonance energies, do not allow us to obtain the value of the S -factor, which would be consistent with previous results. Only a decrease in the resonance width to 22–26 keV leads to the S -factor of the order of 5 keV·b, which is consistent with the upper limit of the results from [26] and the results of other works, for example, [16, 22, 23]. Thus, an accurate determination of the width is crucial. Our results demonstrate that contributions of the $M1$ and $E2$ transitions in the S -factor are negligible at energies $E < 1$ MeV, but are significant at high energies. At the resonance energy, the S -factor reaches 2.4 MeV·b, which is in a good agreement with the results of previous studies. Using the MPCM capabilities, it was shown that the values of the astrophysical S -factor of the $^{13}\text{N}(p, \gamma)^{14}\text{O}$ reaction at ultralow energies strongly depends on the 3S_1 resonance parameters.

Based on the potentials for the S scattering wave, consistent with the energy and widths of the first resonance, the $^{13}\text{N}(p, \gamma)^{14}\text{O}$ reaction rate was calculated and a simple analytical approximation for the reaction rate was proposed. The inclusion of resonances at 1.981, 3.117, and 5.123 MeV practically does not affect the reaction rate, although, the contributions of resonances are clearly visible when calculating the S -factor. The reason for such a weak influence is their small widths and relatively large resonance energies. Results of our calculations for the $^{13}\text{N}(p, \gamma)^{14}\text{O}$ reaction rate provide the contribution to the steadily improving reaction rate libraries.

A precise knowledge of a cross section of the radiative proton capture on ^{13}N isotope at the low energy is important as it plays a key role in the HCNO cycle, due to the proton capture rate on ^{13}N at temperature range of $0.05 T_9 - 1.0 T_9$ can become of the same order or larger than the $^{13}\text{N}(e^+ \nu_e)^{13}\text{C}$ decay rate. Our calculations show that at $T_9 = 0.1$ the ratio of the $^{13}\text{N}(p, \gamma)^{14}\text{O}$ and $^{13}\text{N}(e^+ \nu_e)^{13}\text{C}$ rates is 10.8.

In the context of the CNO cycle scenario, our calculations of the $^{13}\text{N}(p, \gamma)^{14}\text{O}$ and results for the other bottleneck $^{14}\text{N}(p, \gamma)^{15}\text{O}$ reaction [34] together with the NACRE II data [26] for the $^{12}\text{C}(p, \gamma)^{13}\text{N}$ process show that in the temperature window $0.13 < T_9 < 0.97$, where the reaction rate of $^{14}\text{N}(p, \gamma)^{15}\text{O}$ is greater than the reaction rate of $^{13}\text{N}(p, \gamma)^{14}\text{O}$, occurs the conversion of the CNO cycle to the HCNO cycle. The present result indicates that the HCNO cycle is turned on at the early stage of a nova explosion at temperature $T_9 = 0.08$. Therefore, the significant mass flow through ^{14}O nucleus begins to occur at temperature $T_9 = 0.08$. Our calculations show that at this temperature the $^{13}\text{N}(p, \gamma)^{14}\text{O}$ reaction rate and the decay rate of the $^{13}\text{N}(e^+ \nu_e)^{13}\text{C}$ process are equal.

Our results demonstrate that at early stages of a nova explosion at temperatures about $0.1 T_9$ and at late stages of evolution of supermassive stars at temperatures about $1 T_9$ the ignition of the hot CNO cycle could occur at much lower densities of a stellar medium.

Therefore, at temperature and density of a stellar medium such as the conditions in a nova explosion and very massive stars hydrogen burning occurs at temperatures $0.01 T_9 - 1.0 T_9$. For these conditions in CNO cycle the lifetimes of the β^+ -unstable systems such as ^{13}N and ^{15}O are long enough that proton capture can occur on these unstable nuclei before they undergo the β^+ -decay.

Acknowledgement

This work was supported by a grant from the Ministry of Education and Science of the Republic of Kazakhstan under the program # BR05236322 “Investigations of physical processes in extragalactic and galactic objects and their subsystems” under the theme “Study of thermonuclear processes in stars and primary nucleosynthesis of the Universe” through the name of Fesenkov Astrophysical Institute of the National Center for Space Research and Technology of

the Ministry of Digital Development, Innovation and Aerospace Industry of the Republic of Kazakhstan

-
- [1] E. Wiescher, J. Görres, E. Uberseder, G. Imbriani, and M. Pignatari, *Ann. Rev. Nucl. Part. Sci.* **60**, 381 (2010).
- [2] M. Wiescher, F. Käppeler, and K. Langanke, *Ann. Rev. Astron. Astrophys.* **50**, 165 (2012).
- [3] C. R. Brune and B. Davids, *Ann. Rev. Nucl. Part. Sci.* **65**, 87 (2015).
- [4] M. Wiescher, et al., *Nucl. Phys. A* **349**, 165 (1980).
- [5] C. A. Bertulani, A. Gade, *Phys. Rep.* **485**, 195 (2010).
- [6] P. Decrock, Th. Delbar, P. Duhamel, W. Galster, M. Huyse, P. Leleux, I. Licot, et al., *Phys. Rev. Lett.* **67**, 808 (1991).
- [7] P. Decrock, M. Gaelens, M. Huyse, G. Reusen, G. Vancraeynest, P. Van Duppen, et al., *Phys. Rev. C* **48**, 2057 (1993).
- [8] Th. Delbar, W. Galster, P. Leleux, I. Licot, E. Lienard, P. Lipnik, et al., *Phys. Rev. C* **48**, 3088 (1993).
- [9] T.E. Chupp, R.T. Kouzes, A.B. McDonald, P.D. Parker, T.F. Wang, A. Howard, *Phys. Rev. C* **31**, 1023 (1985).
- [10] P. B. Fernandez, E. G. Adelberger, A. Garcia, *Phys. Rev. C* **40**, 1887 (1989).
- [11] M. S. Smith, P. V. Magnus, K. I. Hahn, R. M. Curley, P. D. Parker, T. F. Wang, et al., *Phys. Rev. C* **47**, 2740 (1993).
- [12] T. Motobayashi et al., *Phys. Lett. B* **624**, 259 (1991).
- [13] J. Kiener et al., *Nucl. Phys. A* **552**, 66 (1993).
- [14] G. Baur and H. Rebel, *J. Phys. G.* **20**, 1 (1994).
- [15] Z. H. Li et al., *Phys. Rev. C* **74**, 035801 (2006).
- [16] W. Liu et al., *Int. J. Mod. Phys. E* **15**, 1899 (2006).
- [17] R. J. Charity, K. W. Brown, J. Okolowicz, M. Płoszajczak, J. M. Elson, W. Reviol et al., *Phys. Rev. C* **100**, 064305 (2019).
- [18] P. V. Magnus, E.G. Adelberger, A. Garcia, *Phys. Rev. C* **49**, R1755 (1994).
- [19] G. J. Mathews and F. S. Dietrich, *Astrophys. J.* **287**, 969 (1984).
- [20] K. Langanke, O. S. Van Rognsmalen and W. A. Fowler, *Nucl. Phys. A* **435**, 657 (1985).
- [21] C. Funck and K. Langanke, *Nucl. Phys. A* **464**, 90 (1987).
- [22] X. Tang, A. Azhari, C. Fu, C. A. Gagliardi, A. M. Mukhamedzhanov, F. Pirlepesov, L. Trache, et al., *Phys. Rev. C* **69**, 055807 (2004).
- [23] B. Guo and Z. H. Li, *Chin. Phys. Lett.* **24**, 65 (2007).
- [24] J. T. Huang, C. A. Bertulani, V. Guimarães, *Atomic Data and Nuclear Data Tables* **96**, 824 (2010).
- [25] C. Angulo et al., *Nucl. Phys. A* **656**, 3 (1999).
- [26] Y. Xu, K. Takahashi, S. Goriely et al., *Nucl. Phys. A* **918**, 169 (2013).
- [27] F. Ajzenberg-Selove, *Nucl. Phys. A* **523**, 1 (1991).
- [28] S. I. Sukhoruchkin and Z. N. Soroko, *Excited nuclear states*, Sub. G. Suppl. I/25 A-F. Springer, (2016).
- [29] S. B. Dubovichenko, *Thermonuclear processes in Stars and Universe*. Second English ed., expanded and corrected. Germany, Saarbrücken: Scholar's Press. 2015.
- [30] M. Wiescher and T. Ahn, *Clusters in Astrophysics*, in “Nuclear Particle Correlations and Cluster Physics”, Chap. 8, Ed. Wolf-Udo Schröder, World Scientific, pp. 203-255, 2017.
- [31] S. B. Dubovichenko, *Radiative Neutron Capture*, Walter de Gruyter GmbH, Berlin/Boston, 296 p. (2019).
- [32] S. B. Dubovichenko, A. V. Dzhazairov-Kakhramanov, *Nucl. Phys. A* **941**, 335–363 (2015).
- [33] S. B. Dubovichenko, N. A. Burkova, A. V. Dzhazairov-Kakhramanov, R. Ya. Kezerashvili, Ch. T. Omarov, A. S. Tkachenko, and D. M. Zazulin, *Nucl. Phys. A* **987**, 46 (2019).
- [34] S. B. Dubovichenko, N. A. Burkova, and A. V. Dzhazairov-Kakhramanov, *Int. J. Mod. Phys.* **29**, 1930007 (2020).
- [35] C. A. Barnes, D. D. Clayton, D. N. Schramm, *Essays in Nuclear Astrophysics*. Presented to William A. Fowler. UK, Cambridge: Cambridge University Press. 562p. 1982.
- [36] V. G. Neudatchin, V. I. Kukulín, V. N. Pomerantsev, and A. A. Sakharuk, *Phys. Rev. C* **45**, 1512 (1992).
- [37] O. F. Nemets, V. G. Neudatchin, A. T. Rudchik, Yu. F. Smirnov, Yu. M. Tchuvil'sky, *Nucleon association in atomic nuclei and the nuclear reactions of the many nucleons transfers*. Kiev: Naukova Dumka. 488p. 1988. (in Russian).
- [38] K. Wildermuth and Y. C. Tang, *A unified theory of the nucleus*. Branschweig: Vieweg. 498p., 1977.
- [39] Y. C. Tang, M. LeMere, and D. R. Thompson, *Phys. Rep.* **47**, 167 (1978).
- [40] <https://physics.nist.gov/cgi-bin/cuu/Value?mudjsearch2520for=atomnuc!>
- [41] http://cdfc.sinp.msu.ru/services/ground/NuclChart_release.html
- [42] F. Nichitiu, *Phase shifts analysis in physics*. Romania: Acad. Publ. 416 p. (1980).
- [43] S. B. Dubovichenko, A. V. Dzhazairov-Kakhramanov, *Rus. Phys. J.* **52**, 833 (2009).
- [44] V. G. Neudatchin and Yu.F. Smirnov, *Nucleon associations in light nuclei*. Moscow: Nauka. 414p. 1969. (in Russian).
- [45] C. Itzykson, M. Nauenberg, *Rev. Mod. Phys.* **38**, 95 (1966).
- [46] A. M. Mukhamedzhanov et al., *Nucl. Phys. A* **725**, 279 (2003).
- [47] G. R. Plattner, R. D. Viollier, *Coupling constants of commonly used nuclear probes*, *Nucl. Phys. A* **365**, 8 (1981).
- [48] D. Baye and E. Brainis, *Phys. Rev. C* **61**, 025801 (2000).
- [49] S. G. Ryan and A. J. Norton, *Stellar evolution and nucleosynthesis*, Cambridge University Press, New York, 240 p. 2010.
- [50] <http://cdfc.sinp.msu.ru/exfor/index.php>.
- [51] G. R. Caughlan and W. A. Fowler, *Atom. Data Nucl. Data Tab.* **40**, 283 (1988).
- [52] C. F. von Weizsäcker, *Physikalische Zeitschrift.* **38**, 176 (1937).

- [53] H. A. Bethe, Phys. Rev. **55**, 103 (1939).
- [54] C. Rolfs and W. S. Rodney, *Cauldrons in the Cosmos*, University of Chicago Press, Chicago, 1988.
- [55] M. Wiescher, J. Gorres, F. -K. Thielemann, and H. Ritter, Astron. Astrophys. **160**, 56 (1986).